Atmos. Chem. Phys. Discuss., https://doi.org/10.5194/acp-2018-131
Manuscript under review for journal Atmos. Chem. Phys.
Discussion started: 15 March 2018

Atmospheric Chemistry and Physics
Open Access
Discussions

Extreme temperature and precipitation response to solar dimming and stratospheric aerosol geoengineering

Duoying Ji[1], Songsong Fang[1], Charles L. Curry[2,3], Hiroki Kashimura[4], Shingo Watanabe[5], Jason N. S. Cole[6], Andrew Lenton[7], Helene Muri[8,9], Ben Kravitz[10] and John C. Moore[1,11,12]

[1]College of Global Change and Earth System Science, Beijing Normal University, Beijing 100875, China
[2]School of Earth and Ocean Sciences, University of Victoria, Victoria, British Columbia, Canada
[3]Pacific Climate Impacts Consortium, University of Victoria, Victoria, British Columbia, Canada
[4]Department of Planetology/Center for Planetary Science, Kobe University, Kobe, Japan
[5]Japan Agency for Marine-Earth Science and Technology, Yokohama, Japan.
[6]Canadian Centre for Climate Modelling and Analysis, Environment and Climate Change Canada, Victoria, British Columbia, Canada
[7]Oceans and Atmosphere, Hobart, Tasmania, Australia
[8]Department of Geosciences, University of Oslo, Oslo, Norway
[9]Department of Energy and Process Engineering, Norwegian University of Science and Technology, Trondheim, Norway
[10]Atmospheric Sciences and Global Change Division, Pacific Northwest National Laboratory, Washington, USA
[11]Arctic Centre, University of Lapland, P.O. Box 122, 96101 Rovaniemi, Finland
[12]CAS Center for Excellence in Tibetan Plateau Earth Sciences, Beijing 100101, China

Correspondence to: John C. Moore (john.moore.bnu@gmail.com)

Abstract. We examine extreme temperature and precipitation under two potential geoengineering methods forming part of the Geoengineering Model Intercomparison Project (GeoMIP). The solar dimming experiment G1 is designed to completely offset the global mean radiative forcing due to a CO2-quadrupling experiment (abrupt4×CO2), while in GeoMIP experiment G4, the radiative forcing due to the representative concentration pathway 4.5 (RCP4.5) scenario is partly offset by a simulated layer of aerosols in the stratosphere. Both G1 and G4 geoengineering simulations lead to lower maximum temperatures at higher latitudes, and on land primarily through feedback effects involving high latitude processes such as snow cover, sea ice and soil moisture. Maximum 5-day precipitation increases over subtropical oceans, whereas warm spells decrease markedly in the tropics, and the number of consecutive dry days decreases in most deserts. The precipitation during the tropical cyclone (hurricane) seasons becomes less intense, whilst the remainder of the year becomes wetter. Aerosol injection is more effective

Atmos. Chem. Phys. Discuss., https://doi.org/10.5194/acp-2018-131
Manuscript under review for journal Atmos. Chem. Phys.
Discussion started: 15 March 2018

Atmospheric Chemistry and Physics Discussions

than dimming in moderating extreme precipitation (and flooding), possibly due to stratospheric warming by aerosol injection working in tandem with sea surface temperature reductions to moderate extreme tropical storm cyclogenesis. The differences in the response of temperature extremes between the two types of geoengineering are relatively minor. Despite the magnitude of the radiative forcing applied in G1 being ~6.5 times larger than in G4, and differences in the aerosol chemistry and transport schemes amongst the models, one can discern clear differences in the precipitation extremes between the types of geoengineering probably due to the aerosol direct effect and related energetic changes.

1 Introduction

Global atmospheric greenhouse gas (GHG) concentrations continue to increase due to slow progress in reducing net GHG emissions in the industrialized world. Even if countries with existing commitments reduce emissions to meet their national goals (or aspirational targets under the 2015 Paris Agreement), this may not be sufficient to avoid dangerous or irreversible climate change (Sanderson et al., 2016). Climate engineering is increasingly being discussed as a means to lessen or ameliorate the effects of global warming. In particular, Solar Radiation Management (SRM), the artificial reduction of incoming solar radiation has been increasingly studied: examples include mirrors in space (Mautner, 1989), stratospheric aerosol injection (e.g., Budyko, 1977; Crutzen, 2006) or marine cloud brightening (e.g., Latham, 1990). Scientific investigation of SRM has made use of several different climate models examining various degrees of SRM and greenhouse gas forcing (e.g., Bala et al., 2008; Irvine et al., 2011; Schmidt et al., 2012). While gross features of (for example) global temperature patterns under SRM appear robust, more subtle climate indices require standardized experimental design. Kravitz et al. (2011) defined a set of numerical SRM experiments under the Geoengineering Model Intercomparison Project (GeoMIP), comprising both solar dimming experiments (G1 and G2) and stratospheric aerosol injection simulations (G3 and G4). Marine cloud brightening experiments (G4cdnc, G4sea-salt) were added later (Kravitz et al., 2013c), and initial analysis of these simulations are presented in Ahlm et al. (2017) and Stjern et al. (2017).

The mean climate response under G1 and G2 of diverse climate variables, e.g. temperature, precipitation, sea level pressure has been well described (e.g., Schmidt et al., 2012; Kravitz et al., 2013b; Tilmes et al., 2013; Jones et al., 2013). Curry et al. (2014) drew attention to the changes in temperature and precipitation extremes in models running the reduced solar radiation G1 experiment, and Aswathy et al. (2015) examined extremes under G3 and G3-SSCE (marine cloud brightening by sea salt emission, modelled after GeoMIP experiment G3). Dagon and Schrag (2017) showed that solar geoengineering produces fewer extreme heat events than the future with global warming, though the regional response is variable in part due to varying soil moisture content: soils dry out over the course of the summer as daily maximum temperature increases, and this relationship is strengthened under solar geoengineering. These are the only dedicated analyses of climate model extreme indices under geoengineering to date.

This paper will provide a first look at the difference in the extremes of temperature and precipitation between two geoengineering methods: G1 (solar dimming) and G4 (stratospheric aerosol injection) experiments. That there can be a difference in the mean climate response in reduced solar constant and stratospheric sulphate aerosols has been shown (Yu et al., 2015; Niemeier et al., 2013; Ferraro et al., 2014) and we expect that this will also be evident in the temperature and precipitation extremes. We perform analyses on daily output from GeoMIP models that have completed both G1 and G4, which is a limited subset of models with several excluded from these analyses because only monthly resolution output was saved. We take the results from G1 relative to its corresponding CMIP5 experiment, abrupt4×CO2 to examine impacts of solar dimming, and take the results from G4 relative to rcp45 (the simulations forced by the RCP4.5 scenario) as the impact of stratospheric aerosol injection. The paper is organized as follows: The multimodel ensembles and the definitions of indices are briefly described in Section 2. The probability density functions of monthly mean temperature and precipitation and the results are given in Section 3, along with global mean time series and spatial and seasonal differences of the extreme climate indices in the two SRM experiments. Finally, and a summary of the main findings and conclusion are given in Section 4.

2 Data and Methods

2.1 GeoMIP Experiments

G1 simulates balancing the GHG forcing from the CMIP5 experiment abrupt4×CO2 (instantly quadrupled CO_2 relative to pre-industrial levels) by decreasing solar irradiance. The G1 experiment runs for 50 years beginning from the control run (the piControl scenario; Taylor et al., 2012). The globally averaged top of atmosphere (TOA) radiation differences between G1 and piControl are no more than 0.1 Wm^{-2} (Kravitz et al., 2011). The G1 results can also be naturally compared with results from the abrupt4×CO2 simulation itself, which most model groups have performed (Taylor et al., 2012).

G4 is based on the RCP4.5 future climate scenario (hereafter "rcp45", Meinshausen et al., 2011; Taylor et al., 2012), with additional injection of SO_2 into the tropical lower stratosphere at a rate of 5 Tg per year from the year 2020. The G4 experiments do not specify any specific treatment of chemical or physical properties, so inter-model differences are expected to be larger than in G1 simply from differences in the implementation of the aerosol injection (Kravitz et al., 2011; Yu et al., 2015). The stratospheric injection scenario, G4, is a much smaller signal with respect to its control under the mild GHG forcing specified by RCP4.5 than the G1 experiment with respect to its control abrupt4×CO2.

We analyze the daily output from six Earth system models which completed both the G1 and G4 experiments (Table 1). In order to compare the impacts of the two SRM methods, we also made use of the corresponding outputs from piControl, abrupt4×CO2, and rcp45. We exclude the first decade following the large increase in forcing in common with other authors (Schmidt et al., 2012; Curry et al. 2014), and base our analysis on 40 years of data. All G1 and abrupt4×CO2 simulations are analyzed over a common period of simulation years 11 to 50, and the G4 and rcp45 simulations are analyzed from year 2030 to 2069. Equal weight is given to each model in the analysis.

2.2 Climate extreme indices

Here we use the climate indices defined by the Expert Team on Climate Change Detection and Indices (ETCCDI) (Zhang et al., 2011) to provide a comprehensive overview of temperature and precipitation changes based on daily output of multi-models in GeoMIP and the Climate Model Intercomparison Project Phase 5 (CMIP5; Taylor et al., 2012). These indices have been widely used previously, both for observed weather (Donat et al., 2013) and model output (Tebaldi et al., 2006; Orlowsky and Seneviratne, 2012; Seneviratne et al., 2012) with Curry et al. (2014) using them for G1, Aswathy et al (2015) for G3, and Sillmann et al. (2013b) for CMIP5 models running the RCP scenarios.

We use six indices to describe temperature and precipitation extremes (Table 2), based on the daily output of surface air temperature and precipitation (tasmin, tasmax, pr). TXx and TNn are the maximum daily maximum and minimum daily minimum, respectively, of 2-m air temperature. These are absolute indices, representing the hottest or coldest day of a year or a month. The duration indices CSDI and WSDI are

Atmos. Chem. Phys. Discuss., https://doi.org/10.5194/acp-2018-131
Manuscript under review for journal Atmos. Chem. Phys.
Discussion started: 15 March 2018

the longest number of consecutive days below (exceeding) the 10th (90th) percentiles of daily minimum (maximum) temperatures (Table 2) calculated from piControl and indicate the length of cold spells and warm spells. The precipitation index Rx5day, the maximum 5-day precipitation sum in a month or year, can be taken as a rough indicator of increased flood probability (Frich et al., 2002). CDD is the maximum number of consecutive dry days with precipitation < 1 mm in a year, and is often referred to as a drought indicator.

All model output fields were re-sampled to a median model grid resolution of 144×90 (2.5° longitude × 2° latitude), which corresponds to the grid of the GISS-E2-R model. Following Curry et al. (2014) we adopted a first-order conservative remapping algorithm for non-integer variables (TXx, TNn, and Rx5day), (Jones, 1999), and nearest-neighbour interpolation for integer variables (CSDI, WSDI, and CDD).

3 Results

3.1 Probability distributions of monthly temperature and precipitation

When discussing changes in climate variables the choice of reference scenario is important, though somewhat arbitrary. Curry et al. (2014) chose piControl as the reference for their study of G1, but here we choose abrupt4×CO2 as the reference for G1 and rcp45 as the reference for G4. Our motivation for doing this is that because a return to pre-industrial era is not proposed or even likely to be desirable given the enormous quantities of GHG that would need to be removed from the climate system, in reality we will have to choose between either a world with GHG forcing, or with GHG forcing plus geoengineering. Atmospheric CO_2 concentrations equal those in abrupt4×CO2 would be reached by about the year 2100 under business-as-usual scenarios like RCP8.5. We computed the probability density functions (PDFs) of temperature and precipitation for all models to get a general idea of the changes in the two geoengineering experiments (G1 and G4) compared to their baseline experiments (abrupt4×CO2 and rcp45). We first calculated the standardized monthly anomalies of monthly mean surface temperature in abrupt4×CO2 at every grid point in each model, i.e.

$$\tau_m^{ref} = (T_m^{ref} - \overline{T}_m^{ref}) / \sigma_{T_m}^{ref}$$

where an overbar denotes the means of each month of the year calculated for the 11th to 50th years of the simulations and $\sigma_{T_m}^{ref}$ is the similarly calculated standard deviation for month m in the reference experiment, abrupt4×CO2 or rcp45. Next, we computed the monthly anomalies in G1 and G4 relative to the reference mean and standard deviation, i.e.

$$\tau_m^{Geo} = (T_m^{Geo} - \overline{T}_m^{ref})/\sigma_{T_m}^{ref}$$

The same algorithm was used to generate PDFs of precipitation. The multi-model mean PDFs use equal weights for each model. The results are shown in Figure 1. The PDFs for G1 and abrupt4×CO2 differ from those presented by Curry et al. (2014) due to the different choice of reference simulation.

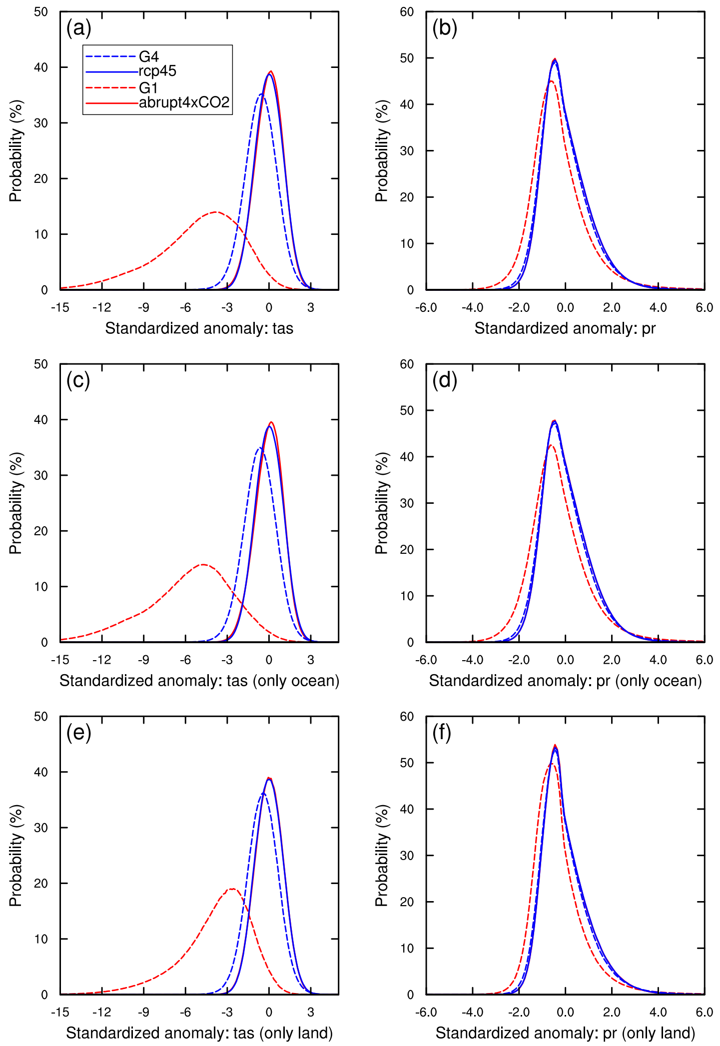

Figure 1: Probability density distributions, normalized to 100%, of standardized monthly mean anomalies for the model ensemble average for four experiments: abrupt4×CO2 (solid red line), G1 (dashed red line), rcp45 (solid blue line), and G4 (dashed blue line). The PDFs of surface air temperature are shown in the left-hand panels, precipitation in the right-hand panels. Upper panels show global results, middle panels ocean-only, and lower panels land-only. Tas denote surface air temperature, while pr denotes precipitation.

The PDFs of global temperature (i.e., including all points on each model grid; Fig 1a) show a dramatic negative shift in G1 experiment, indicating cooling at nearly all locations in the models compared with abrupt4×CO2. Under G4 the PDFs display discernible differences from rcp45, mainly as negative anomalies—but the change is much smaller in G4-rcp45 than in G1-abrupt4×CO2. The relationships remain the same over the ocean and land domains as in the global. Figures 1c and 1e reveal that differences between temperature extremes over ocean and land domains are small, but the PDFs are more strongly centrally peaked over land than over ocean.

The PDFs of monthly precipitation display smaller differences between the two experiments than for temperature (right-hand panels of Fig.1). The PDFs are positively skewed in all cases, a general characteristic of precipitation and other positive definite climate variables (e.g., wind speed). The largest difference between G1 and abrupt4×CO2 occurs over ocean, where low tails are shifted towards more negative precipitation anomalies in G1 (Fig. 1f). As in the case of temperature, changes under G4-rcp45 are much smaller than under G1-abrupt4×CO2 with only a slight negative shift. Fig.1d & f show that there are almost no differences between G4 and rcp45 over both land and ocean.

3.2 TOA net shortwave radiation

G1 introduces ~ -11.1 Wm^{-2} shortwave radiative forcing, whereas G4 implies ~ -1.7 Wm^{-2} reduction, hence the ratio between them is a factor of ~ 6.5, but the spatial distribution of net shortwave radiation flux anomalies at the top of atmosphere (TOA) for the G1 and G4 ensemble means are quite similar (Figure 2). However, differences are clearer when we investigate the spatial pattern of the ratio between the two SRM experiments, with most regions having a ratio between 5 to 7, although there are large inter-model differences. Some models (BNU, GISS), and the entire ensemble, show a small ratio about ~1 east of Greenland in the North Atlantic, the region associated with the overturning part of the Atlantic meridional circulation (AMOC), and which under the G1 forcing was shown to be strongly affected by changes in radiative forcing and air/ocean heat exchange (Hong et al., 2017). In contrast many equatorial regions show larger ratios, up to 15. In some models, the Southern Ocean and the Intertropical and South Pacific Convergence Zones also display low ratios. These results suggest that dimming and aerosol geoengineering forcing may affect clouds differently in some models: low level clouds are important for radiative surface fluxes in the North Atlantic and Southern Ocean where ratios between G1 and G4 are close to 1, while higher clouds are more important in the deep tropical convection regions where ratios are much higher. The models show less consistent responses under both G1 and G4 SRM over Southern Ocean around Antarctica, where CMIP5 models also show large uncertainties on cloud radiative effects

(Stocker et al. 2013). It is also possible that surface albedo changes due to sea ice and snow cover are responsible for the large differences in net shortwave flux in the coastal Antarctic seas, and the more modest differences seen in the North Atlantic and Barents Sea along with Alaska and eastern Siberia.

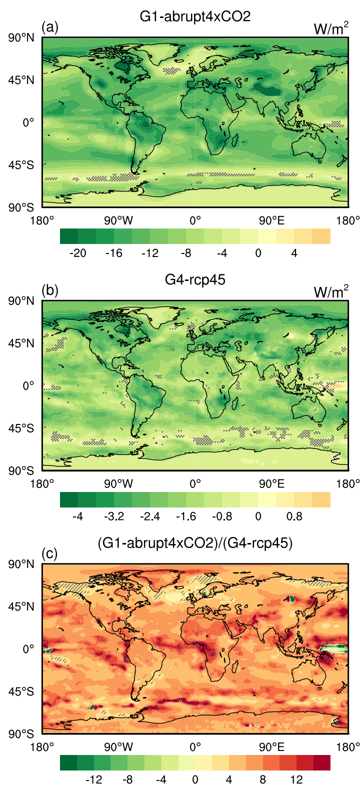

Figure 2: Geographical distributions over the 40-year analysis periods of differences in shortwave radiation flux at TOA between G1-abrupt4×CO2 (top), G4-rcp45 (middle), (G1-abrupt4×CO2)/(G4-rcp45) (bottom). In (a) and (b) stippling indicates regions where fewer than 5 of 6 models agree on the sign of the model response. Note that all three panels have different scales. In (c), hatching indicates significant change larger than the 95th or smaller than the 5th percentile threshold value.

3.3 Global mean time series

Figure 3 shows the differences (Δ) G1-abrupt4×CO2 and G4-rcp45 for TXx and TNn. In G1-abrupt4×CO2, ΔTNn is significantly negative (Fig.3a), with a multimodel mean value of −5.1±0.4 °C (one standard deviation, Table 3) over the 40 years analysis period (shaded region in Fig. 3a). By contrast, the extreme temperature index TXx has a smaller decrease with mean differences of -4.4±0.3 °C. Multi-

Atmos. Chem. Phys. Discuss., https://doi.org/10.5194/acp-2018-131
Manuscript under review for journal Atmos. Chem. Phys.
Discussion started: 15 March 2018

model mean values of ΔTNn are consistently a factor of ~1.2 more negative than those of ΔTXx (Fig. 3a and c), indicating a much stronger response of night-time low temperatures to a reduction in the solar constant, relative to daytime high temperatures. This is also the case in G4-rcp45, but with much smaller magnitude (ΔTNn = -0.7±0.1 °C and ΔTXx = -0.6±0.1 °C), Figs. 3b, d. The larger change in TNn relative to TXx was also found in the GeoMIP G1-piControl simulations analyzed by Curry et al. (2014), and in the increasing GHG scenarios in CMIP3 as well as CMIP5 (Tebaldi et al., 2006; Orlowsky and Seneviratne, 2012; Sillmann et al., 2013a). The explanation for the difference in daytime and night-time response is due to much stronger response of night-time low temperatures than daytime high temperatures. TNn is reduced more than TXx under G1 (and G4) because of the reduced warming under geoengineering, lower temperatures and reduced longwave effects throughout the whole day and night, although the reduced shortwave surface heating impacts daytime temperatures directly under G1 (and G4). The GISS-E2-R model has a noticeably weaker response measured by ΔTNn and ΔTXx changes than the other models. This is due to its relatively weak warming under abrupt4×CO_2 as shown by Curry et al. (2014), meaning that the degree of solar dimming needed by G1 SRM is also weaker than for other models. The changes in radiative forcing at both short and long wavelengths are thus smaller in GISS-E2-R and the changes in various climate indicators are also smaller (Yu et al., 2015).

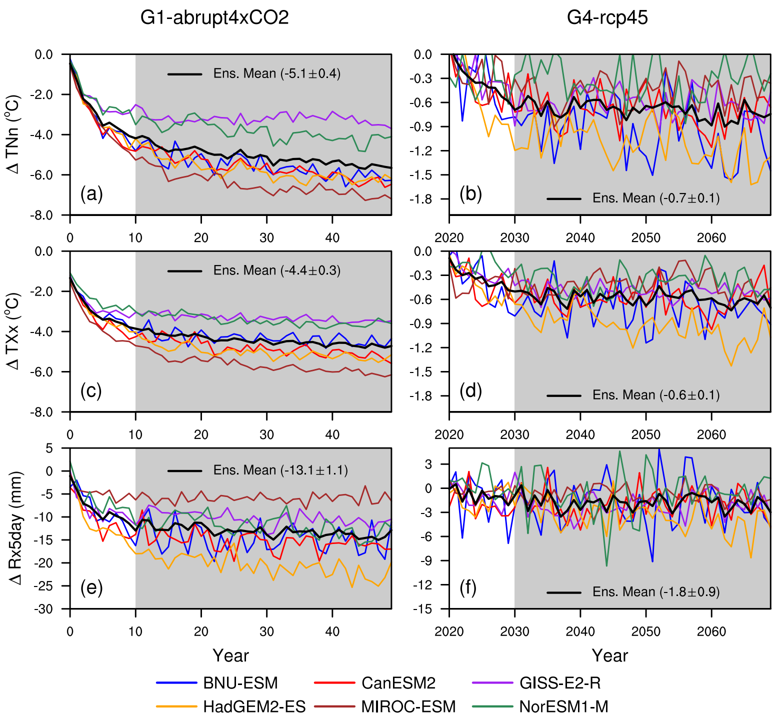

Figure 3: Time series of the difference of global mean extreme indices (as labelled on each left-hand panel's ordinate) between G1 - abrupt4×CO2 (left column) and G4 - rcp45 (right column) for all models analyzed. The black curves are the multimodel means, and gray shading indicates the 40-year analysis period for each experiment used in this study, with the ensemble mean value also shown on each panel.

The corresponding result for the extreme precipitation index, Rx5day is a significant reduction under G1 (Fig.3e) with a multi-model mean value of -13.1±1.1 mm, indicating an overall weakening of the hydrological cycle. This feature was noted for non-extreme indices in the G1 experiments analyzed by Schmidt et al. (2012) and Kravitz et al. (2013b). In contrast, the index for G4-rcp45 (Fig.3f) is near-zero though slightly negative on the whole, with the multi-model mean value of -1.8±0.9 mm. The mean temperature difference under G1 SRM is -4.3 °C, and -0.5 °C under G4 aerosol SRM, hence a ratio of 8.1, larger than extreme aspects of temperature: 7.3 for TNn, and 7.6 for TXx (Table 3). The corresponding ratio for mean precipitation is 7.0, whereas extreme precipitation indicated by Rx5day has a ratio of 7.3., similar to TNn and TXx. If relative humidity and atmospheric circulation remain relative unchanged then intense precipitation amount is governed by total precipitable water in the atmosphere, which the Clausius-Clapeyron relation says scales with mean temperatures. This would imply the ratios

Atmos. Chem. Phys. Discuss., https://doi.org/10.5194/acp-2018-131
Manuscript under review for journal Atmos. Chem. Phys.
Discussion started: 15 March 2018

Atmospheric Chemistry and Physics
Discussions

of extreme precipitation and mean temperatures would be the same between the G1 and G4 experiments. This is not the case here where extreme precipitation scales with extreme temperature. This suggests that simple scaling arguments do not capture the full differences in the response to different types of geoengineering, and that there are likely changes in atmospheric circulation (or relative humidity) that need to be considered as well. Solar dimming SRM and stratospheric aerosol SRM seem equally effective at changing extreme precipitation as well as extreme high and low temperatures, though solar dimming SRM seems more effective than stratospheric aerosol SRM at controlling mean temperature.

3.3 Spatial Response in Extremes

Geographical patterns of difference between the two SRM scenarios: i.e., G1- abrupt4×CO2 and G4-rcp45 are shown in Figure 4.

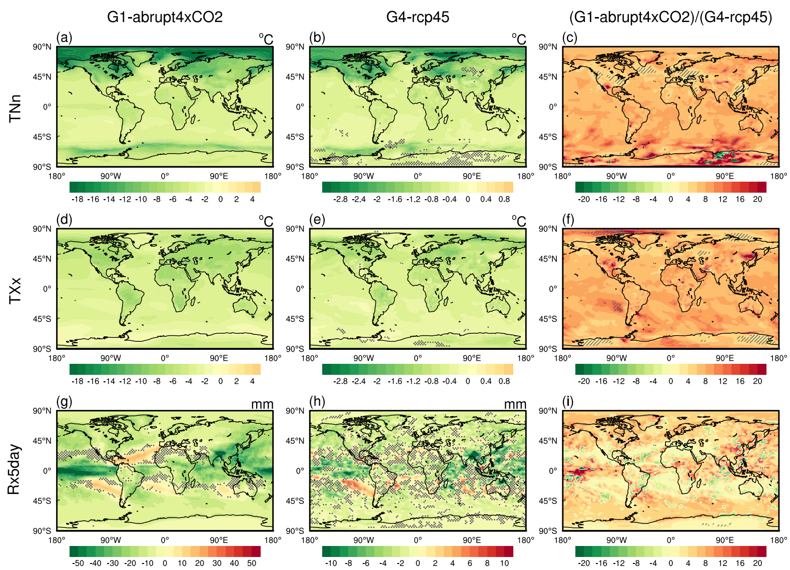

Figure 4: Geographical distributions over the 40-year analysis periods of the differences G1 - abrupt4×CO2 (left column), G4 - rcp45 (middle column), and (G1 - abrupt4×CO2)/(G4 - rcp45) (right column) for the extreme indices TNn (top row), TXx (middle row), and Rx5day (bottom row). Panel (i) is the ratio of one-percentage of Rx5day range binned values rather than absolute values of Rx5day to avoid large changes for near zero values. Stippling in the left and middle columns indicates regions where fewer than 5 of 6 models agree on the sign of the model response. In the right column, hatching indicates significant change (larger

than the 95th or smaller than the 5th percentile threshold value). Note that colour bars of left and middle columns have different scales.

The cooling patterns seen for TNn (Fig.4a,b) are similar but with a larger signal for G1-abrupt4×CO2 than G4-rcp45, with the signature of polar amplification evident in both hemispheres but primarily in the Arctic. Similar patterns occur in simulations of mean temperatures under both GHG warming scenarios and under geoengineering scenarios (Schmidt et al., 2012; Curry et al., 2014; Kravitz et al., 2013b). Pithan and Mauritsen (2014) conclude that in climate models it is primarily the temperature feedback with surface albedo of secondary importance in producing Arctic amplification under GHG forcing. While James et al. (2010) concluded that changes in sea ice cover play a leading role in recent Arctic temperature amplification for GHG forcing. The spatial pattern under geoengineering is due to the seasonal differences in longwave and shortwave forcing. Tilmes et al., (2014) and Hong et al., (2017) note the importance in poleward heat transport by reduction in the strength of the meridional overturning circulation under GHG forcing. Geoengineering has been shown to mitigate sea ice loss (Moore et al., 2014; Berdahl et al., 2014), and also reduce the decline in ocean poleward heat transport (Hong et al., 2017) relative to GHG forcing, but these changes do not completely counter the increase in radiative flux due to GHG forcing.

A notable feature is the larger cooling over land compared with oceans, also expressed in Table 3. Under GHG warming scenarios, opposite differences are due to heat capacity differences, contrasts in surface sensible and latent fluxes, and also to boundary layer differences (Sutton et al., 2007; Joshi et al., 2008). The land–sea cooling contrast is also sensitive to stratospheric aerosol forcing as is shown under G4-rcp45 (Fig 4b,4e). This is consistent with Volodin et al. (2011) who found increased land–sea cooling contrast in annual mean temperature using the INMCM model forced with 4 Mt S/year equatorial stratospheric aerosol injection. The land-sea cooling contrast is larger for TXx than TNn (Fig 4d, e; Table 3), consistent with the stronger relationship of shortwave forcing to TXx.

Comparing Figs. 4a,b and d,e shows that the magnitude of ΔTNn is larger than that of ΔTXx at high latitudes. The strongest cooling in TXx of up to -9.9°C under G1-abrupt4×CO2 (Fig. 4d) generally occurs in the interior of the continents as previously discussed, such as in South and North America, Eastern Europe, north-central Eurasia and Australia. The pattern is similar in G4-rcp45 except in eastern China, where reduced solar radiation produces more cooling than aerosol injection relative to adjacent regions (Fig. 4f). Fig. 4c, f show the ratio of the changes G1-abrupt4×CO2 to G4-rcp45. Averaged over the globe, the magnitude of the extreme temperature anomalies under G1-abrupt4×CO2 is a factor of ~8 larger than under G4-rcp45, simply due to the much larger forcings in G1 relative to G4 (Table 3). Significantly smaller ratios for ΔTNn occur in central North America, eastern China and the northern Mediterranean as well as areas in Antarctica, with significantly larger ratios mainly in the Southern Ocean. Corresponding results for ΔTXx show smaller ratios in northern North America and Asia, West Asia, as well as areas in Antarctica, with larger ratios mainly in northeastern China and southern North America as well as in some ocean areas.

Using geoengineering to alleviate surface warming from increasing GHGs concentrations decreases global-mean precipitation (Schmidt et al., 2012; Kravitz et al., 2013b) as well as the wettest five days index (Rx5day), representing an extreme aspect of the precipitation distribution (Curry et al., 2014). The ensemble means, expressed in percentage terms, show that Rx5day is strongly reduced over high latitudes and equatorial regions, especially in the equatorial Pacific and polar regions, where reductions of up to 126mm occur. This is due to increased atmospheric stability and suppression of convection under geoengineering (Bala et al.,2008). Fig. 4g and Curry et al. (2014) show some robust increases in the tropics, northwest Africa, the Mediterranean Sea and areas of the subtropical oceans, which consistently display decreased Rx5day under abrupt4×CO2 compared to G1. This has been attributed to a weaker Hadley cell due to weaker radiative forcing, (Tilmes et al., 2009), but more recent analysis of the tropical circulation (Davis et al., 2016; Smyth et al., 2017; Guo et al., submitted to ACP) suggest more complex interactions between radiative forcing and Hadley cell extent and intensity. The spatial pattern for G4-rcp45 is not as coherent as that for G1-abrupt4×CO2, although Rx5day also increases mainly in the subtropics and decreases at high latitudes and over most land areas (Fig. 4h). The noisy G4-rcp45 response is also seen in the climatological mean precipitation (Yu et al.,2014) under G3 and G4, as well as in the consecutive dry days (CDD) index under the G3 experiment (Aswathy et al., 2015). Furthermore, monsoonal regions including East Asia and India exhibit negative changes under G1-abrupt4×CO2, which may be attributed to a weakened monsoon. Tilmes et al. (2013) observed, using a larger ensemble of models, that G1-abrupt4×CO2 results in a robust decrease in monsoonal precipitation, while it increases under abrupt4×CO2. However, the change under G4-rcp45 is not as robust, at least partially due to the lowered mean temperature changes and land-sea thermal contrast response to the stratospheric aerosol injection.

We compared tropical (± 30º lat.) relative frequency changes of four major daily rain types: light rain (<0.3 mm/day), moderate rain (0.9–2.4mm/day), heavy rain (>9mm/day) and an extremely heavy rain type (>24 mm/day) according to daily rain types used in Lau et al. (2013). All six models show consistent shift in rain regime, with a decrease in the frequency of extremely heavy rain by -22.3% for G1 and -3.6% for G4, heavy rain by -5.2% for G1 and -0.6% for G4, and consistent increase in the frequency of light rain by +4.4% for G1 and 0.5% for G4.

3.4 Extreme Duration Response

The TXx, TNn and Rx5day indices discussed above all characterize aspects of the absolute magnitude of climate extremes. We now analyze the duration indices shown in Figure 5: cold spell duration (CSDI), warm spell duration (WSDI), and consecutive dry days (CDD).

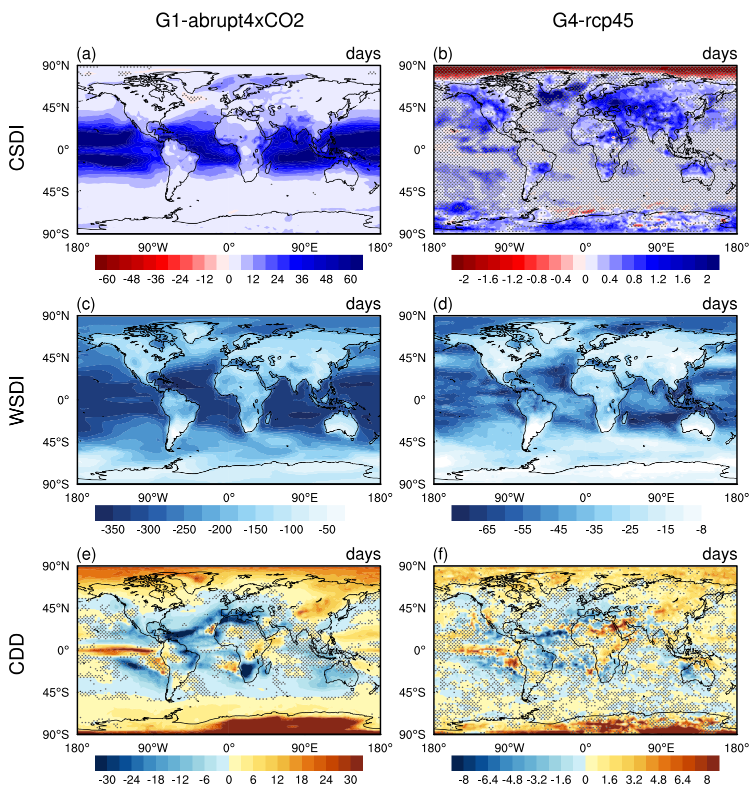

Figure 5: Geographical distributions of differences, G1 - abrupt4×CO2 (left column) and G4 - rcp45 (right column) for the extreme duration indices (a, b) CSDI, (c, d) WSDI, and (e, f) CDD, taken over the 40-year analysis periods. Stippling indicates regions where fewer than 5 of 6 models agree on the sign of the model response.

CSDI increases worldwide in the G1-abrupt4×CO2 anomaly (Fig. 5a), due to the strong negative shift of the PDF of surface temperature for G1 relative to abrupt4×CO2 (Fig. 1a). The most striking feature of Fig. 5a is the robust increase in CSDI over the tropical oceans with ΔCSDI exceeding 50 days per year over large regions, indicating that the region is sensitive to reduced solar radiation. Most of the CSDI differences over land in G1-abrupt4×CO2 are robust, with the notable exception of tropical regions such as India and Indonesia, which experience an increase in cold spell duration of more than 30 days (Fig. 5a). In contrast to the large response under G1-abrupt4×CO2, the pattern in G4-rcp45 is incoherent with wide disagreement about the sign of change between the models except for a robust increase over the continental regions of Eurasia and North America.

The spatial pattern of WSDI (Fig. 5c) shows a notable decrease over the tropical oceans, exceeding 300 days per year. The pattern is similar to CSDI but of larger magnitude and with a more widespread decrease over land areas such as eastern south America and the Tibetan Plateau (Fig. 5c). Comparison of Figs. 5a and 5c shows that in G1-abrupt4×CO2, WSDI decrease much more strongly over the tropical and subtropical oceans than do CSDI. The pattern of WSDI in G4-rcp45 is similar to that in G1-abrupt4×CO2, except in the equatorial ocean regions, which is also noticeable in the pattern of changes in CSDI (Figs. 5a, b).

The relatively small, but robust, changes in annual extreme temperature in the tropics apparently contradict the rather large robust increases in CSDI and decreases in WSDI (Fig. 5a, c) under solar dimming, but were also reported by Curry et al (2014). Cold spell and warm spell duration are related to the magnitude of changes in mean temperature relative to the short-term temperature variability. They are sensitive to the underlying climatological temperature variability of the respective region (Radinovio et al., 2012), which is small in the tropics and larger in the extra-tropics. A small shift in mean temperature can lead to large changes in the duration of cold and warm spells, which may have relatively large impacts on ecosystems (Corlett, 2011). The more robust results (lack of stippling in Fig. 5d) for the WSDI anomalies under G4 than for the CSDI are due to the significant cooling imparted by G4 relative to rcp45, as reflected by the color bar ranges. For example, BNU-ESM shows small increases in CSDI over the Arctic Ocean, while HadGEM2-ES shows strong decreases and other models have spatially varying results in G4 relative to rcp45. This may be due to Arctic amplification linked to, among other things discussed in Section 3.3, loss of sea ice, which occurs under both rcp45 and G4 simulations (Berdahl et al., 2014). There is a wide model spread in model-projected Arctic sea ice extent, although HadGEM2-ES and BNU-ESM produce similar sea ice patterns while MIROC-ESM simulates essentially no ice cover in autumn (Berdahl et al., 2014).

The equatorial Pacific in the vicinity of the inter-tropical convergence zone (ITCZ) displays increases in CDD under G1-abrupt4×CO2 at the same locations (Fig. 5e) as Rx5day decreases (Fig. 4h). This may be related to the reduced latitudinal extent of seasonal movement of the ITCZ under G1 noted by Smyth et al. (2017). Anticorrelation between CDD and Rx5day can also be seen for decreases in CDD and increases in Rx5day in the South Atlantic and tropical Atlantic; both northern and southern high latitudes also display this pattern. The pattern is especially noticeable in the desert regions of North Africa, Southwest Africa, Australia and Southwest North America which are strongly influenced by the descending branch of the tropical Hadley cell. This implies most places have fewer droughts under the geoengineering simulation than without it. However, the deserts of central Asia exhibit increasing CDD accompanied by decreasing Rx5day. Fig.5f shows that the pattern in G4-rcp45 is similar to G1-abrupt4×CO2 but more noisy.

3.5 Seasonality and zonal mean changes

We now examine the zonal structure and seasonality of changes in the climate extreme indices. Seasonal analysis is performed only for indices that can be presented on a monthly basis, i.e., TXx, TNn, and Rx5day. There are large temperature differences between G1 and abrupt4×CO2 simulations over polar regions due to residual polar amplification effects, and similarly for G4-rcp45 but with smaller magnitude. To aid the comparisons, we normalize the zonal mean difference in the climate extreme indices relative to the global mean difference, i.e.:

$$< \mathrm{X}^{\mathrm{Geo}} - \mathrm{X}^{\mathrm{ref}} >= \frac{\overline{\mathrm{X}}^{\mathrm{Geo}}_{\mathrm{zonal}} - \overline{\mathrm{X}}^{\mathrm{ref}}_{\mathrm{zonal}}}{|\overline{\mathrm{X}}^{\mathrm{Geo}}_{\mathrm{global}} - \overline{\mathrm{X}}^{\mathrm{ref}}_{\mathrm{global}}|}$$

where the operator <> denotes the normalized zonal mean, X is TXx, TNn or Rx5day, an overbar denotes the average over zonal or global, the absolute operator || in the denominator of the right term preserves the sign of the geoengineering anomaly.

Atmos. Chem. Phys. Discuss., https://doi.org/10.5194/acp-2018-131
Manuscript under review for journal Atmos. Chem. Phys.
Discussion started: 15 March 2018

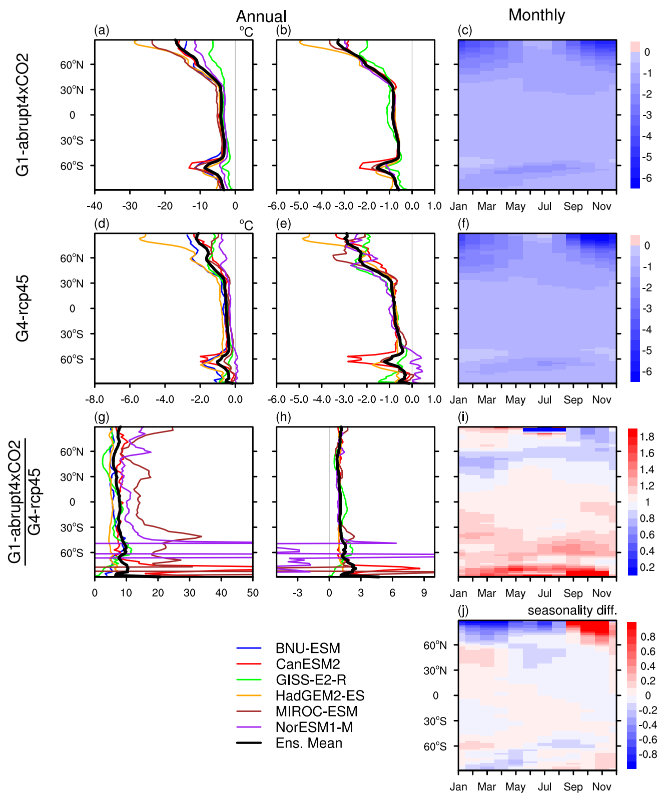

Figure 6: Absolute difference of annual zonal mean in the extreme low temperature TNn (left column), Normalized difference with respect to annual zonal mean (middle column) and monthly zonal mean (right column) in TNn: (a), (b), (c) G1 – abrupt4×CO2, (d), (e), (f) G4 – rcp45, (g), (h), (i) the ratio between G1 – abrupt4×CO2 and G4 – rcp45 taken over the 40-year analysis period, (j) the difference between (c) and (f) with their respective annual zonal means removed. In panel (j) red colours thus indicate relatively greater changes with G4 and blue colours with G1. 3×3-point smoothing was applied to the seasonal-latitude change.

The left panels in Figure 6 display the zonal and annual mean anomalies, ΔTNn. The response in G1 compared with abrupt4×CO2 is of course uniformly negative (Fig. 6a), with multi-model mean annual peak values of -17°C near 90°N and -8°C near 65°S. In G4-rcp45, most models simulate a much smaller negative response.

As shown in the right panels of Fig. 6, the Arctic (defined as the region north of 67.5°N) cooling of TNn has a distinct seasonal character under both G1-abrupt4×CO2 and G4-rcp45. Arctic amplification peaks (up to -25°C in G1-abrupt4×CO2, and -5°C in G4-rcp45, not shown) in early winter (November to December). In winter under abrupt4×CO2, the warm ocean forms only limited seasonal sea ice cover and produces low cloud cover increasing downward longwave radiation and hence remains relatively warm. However, under G1-abrupt4×CO2, the sea ice cover is largely multi-year (Moore et al., 2014), hence is thicker and maintains a much lower surface temperature as the ice cover cools compared with open ocean. In summer, surface melting on the ice, which is still present in most models under abrupt4×CO2, and the large thermal inertia of the ocean tend to drive minimum surface temperatures under both G1 and abrupt4×CO2 close to the freezing point. A distinct TNn decrease is observed in the high latitudes of the Southern Ocean from April to October in both G1-abrupt4×CO2 and G4-rcp45, likely also due to sea ice processes. In G4-rcp45, the pattern is a weaker version than in G1-abrupt4×CO2, by a factor of 7 to 9.

Fig. 6b, 6e show normalized zonal and annual mean anomalies of ΔTNn. Although G1 and G4 possess different geoengineering radiative forcings, the normalized zonal and annual mean anomalies of ΔTNn display similar patterns and magnitudes. The ratio of normalized response in TNn in Fig. 6h is remarkably spatially uniform, and close to unity in the annual mean, except for the high latitudes of the Southern Hemisphere. This is consistent with Fig. 6g, which shows the absolute ratio of response in TNn, and which implies that a constant scaling of the zonal and annual mean response to G4 would be close to that of G1. Hence, in Fig. 6i, values above one indicate where G1 is an intrinsically stronger geoengineering agent than G4, and values less than one highlight where aerosols tend to be more effective, with a value of one meaning that dimming and aerosols are equally effective. Fig. 6i shows that TNn in the northern high latitude summers is affected much more by solar dimming than by aerosol injection. A similar but weaker response is also present in the summertime Southern Ocean. The only regions where aerosol injection induces a significantly larger response than solar dimming is in the high Arctic in winter, suggestive of a longwave radiative effect with aerosols.

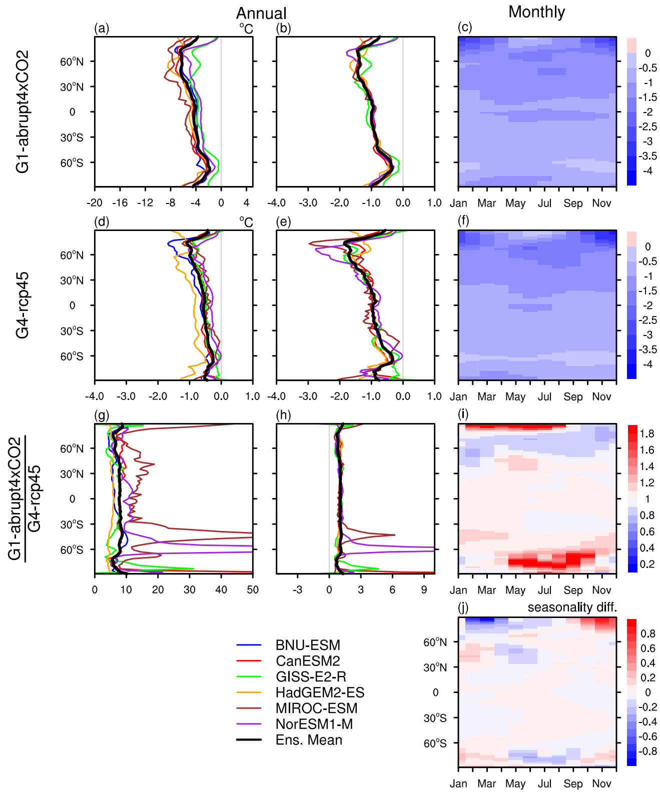

Figure 7: Absolute difference of annual zonal mean in the extreme high temperature TXx (left column), Normalized difference with respect to annual zonal mean (middle column) and monthly zonal mean (right column) in TXx: (a), (b), (c) G1 – abrupt4×CO2, (d), (e), (f) G4 – rcp45, (g), (h), (i) the ratio between G1 – abrupt4×CO2 and G4 – rcp45 taken over the 40-year analysis period, (j) the difference between (c) and (f) with their respective annual zonal means removed. In panel (j) red colours thus indicate relatively greater changes with G4 and blue colours with G1. 3×3-point smoothing was applied to the seasonal-latitude change.

Figure 7 shows that the multi-model mean ΔTXx in both G1−abrupt4×CO2 and G4−rcp45 are of smaller magnitude than ΔTNn at high latitudes (Fig. 6). TXx is much less latitudinally variable than TNn both in G1-abrupt4×CO2 and G4-rcp45 (compare Figs. 6a, d and 7a, d). The signature of polar amplification (especially in the Northern Hemisphere) is evident in ΔTNn (Fig. 6a, d) whereas an asymmetric north – south response is evident for ΔTXx. The north-south ΔTXx asymmetry reflects the global land distribution, with ΔTXx more strongly affected over land than ocean (Fig. 4 d, e). The strongest cooling in G1-abrupt4×CO2 is found in Arctic winter, when more winter Atlantic cyclones track into the high Arctic under abrupt4×CO2 than G1 (Moore et al. 2014), and in the Northern mid-latitude summers, consistent with the regions where snow-albedo feedback and the soil moisture effect are strongest (Orlowsky and Seneviratne, 2012; Seneviratne et al., 2006; Diffenbaugh et al., 2007). Geoengineering leads to increases in both snow cover and soil moisture which lowers surface sensible heat flux, raises heat capacity and thus lowers sensitivity of temperature to radiative forcing changes (Curry et al., 2014, Dagon and Schrag, 2017). Similar patterns hold for G4-rcp45. As with TNn in Fig. 6h, the ratio of normalized response in TXx is remarkably spatially uniform and around one (Fig. 7h). Fig. 7i suggests that relative effectiveness of aerosols and solar dimming is similar, except for the Arctic, and perhaps Antarctic, when aerosols appear more effective than dimming in winter. Since the lack of shortwave radiative forcing during winter would not lead to differences in solar dimming or aerosol response, atmospheric circulation changes are implicated. This may indicate a difference in the GHG responses between abrupt4×CO2 and rcp45 since a strengthening of the wintertime stratospheric polar vortices occurs under GHG forcing, tending to cool polar surface temperatures. This also promotes heterogeneous reactions on aerosols depleting stratospheric ozone, further strengthening the stratospheric vortex and cooling the poles (Tilmes et al., 2009), although this effect is not included in the models used in this study.

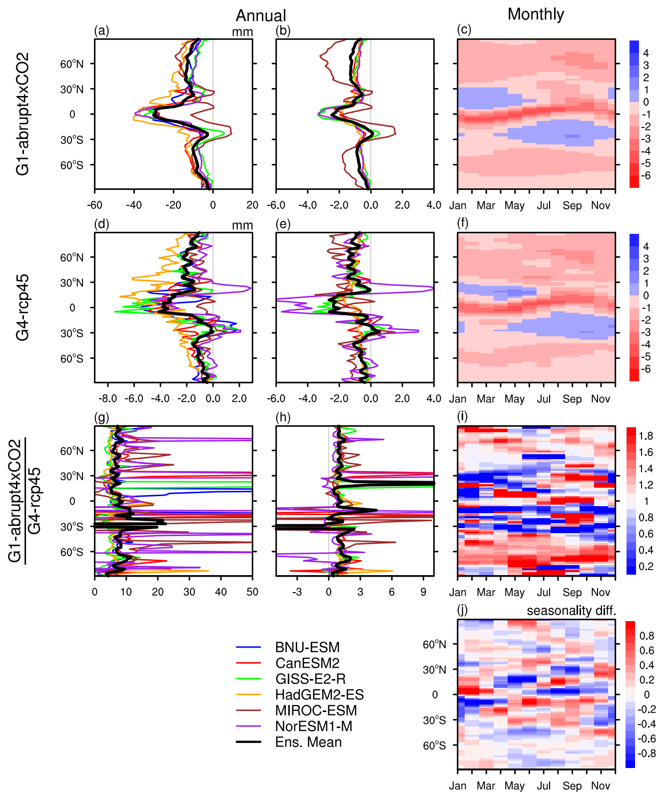

Figure 8: Absolute difference of annual zonal mean in the extreme precipitation Rx5day (left column), Normalized difference with respect to annual zonal mean (middle column) and monthly zonal mean (right column) in Rx5day: (a), (b), (c) G1 – abrupt4×CO2, (d), (e), (f) G4 – rcp45, (g), (h), (i) the ratio between G1 – abrupt4×CO2 and G4 – rcp45 taken over the 40-year analysis period, (j) the difference between (c) and (f) with their respective annual zonal means removed. In panel (j) red colours thus indicate relatively greater changes with G4 and blue colours with G1. 3×3-point smoothing was applied to the seasonal-latitude change.

The results for the extreme precipitation index Rx5day are shown in Figure 8. Under GHG forcing alone, both observations and simulations show wet seasons get wetter and dry seasons get drier (Chou et al., 2013). The months July-November in the Northern Hemisphere and February-March in the Southern Hemisphere become somewhat drier (10-16%) under geoengineering. Fig. 8f displays a similar summer/winter, tropical wet/dry season effect for G4, where it appears over a slightly narrow latitude range and is slightly delayed relative to G1. Increased occurrence of extreme rainfall under G1 (>16%)

is expected during winter and spring for the subtropical regions of both hemispheres. The effect on Rx5day is largest in April to November in the Southern Hemisphere, which roughly corresponds with the subtropical wet season. The path of darker red in Figs 8c and 8f appear to follow quite closely the seasonal migration of the ITCZ which wanders near the sub-solar point. Smyth et al. (2017) report that the seasonal amplitude of migration of the ITCZ is reduced under G1 relative to piControl and this would be consistent with the seasonal reduction in Rx5day along the dark red paths in Figs 8c and 8f. Tilmes et al. (2013) noted that in the G1 experiment precipitation in the tropics is reduced by around 5% with a larger interannual variability and spread among the models over land compared to the ocean. Furthermore there is considerable reduction in frequency of heavy precipitation (> 8 mm day^{-1}) over the tropics and at the same time an increase in the frequency of small and moderate precipitation intensity. This is consistent with the seasonal analysis shown in Fig. 8 if the extreme precipitation events are generally occurring in the wet season, while the small and moderate events primarily occur in the dry seasons.

Prominent decreases in Rx5day are observed year-round at high latitudes consistent with general drying under both geoengineering scenarios. Fig. 8g, 8h shows that the zonal means are noisier than for TNn and TXx. The results look much more complex than the temperature extreme indices in Fig. 6h and 7h. The general effect is that the tropical regions (30ºS-30ºN) are more strongly affected by aerosol injection than by solar dimming, while at other latitudes, dimming is more effective. Ferraro et al. (2014) found that the tropical overturning circulation weakens in response to geoengineering with stratospheric sulphate aerosol injection due to radiative heating from the aerosol layer, but geoengineering simulated as a simple reduction in total solar irradiance do not capture this effect. Mid-latitude Rx5day is more effectively changed by aerosols year-round, while at high latitudes winter solar dimming is effective year-round, and more effective than aerosols during winters. This difference in the ratios in winters when incoming solar radiation is minimal suggests a role for the changes in the stratospheric vortex as discussed above for the spatial differences in TXx.

Stratospheric sulphate aerosols result in heating of the stratosphere, particularly in the tropics, (e.g., Tilmes et al., 2009). Changes in heating rates in the stratosphere and at the tropopause would directly change the tropospheric lapse rate, likely altering the stability of the atmosphere, relative humidity and hence the hydrological cycle. The Northern Hemisphere peak tropical cyclone (TC) season is August through October, and the Southern Hemisphere season is January through March. Interestingly, the Southern Hemisphere ocean basins (5-20°S) where TCs are generated are blue in Fig. 8j during the TC season, while in the Northern Hemisphere the TC basins are red in their TC season. This suggests a dichotomy between the hemispheres insofar as the type of geoengineering that may moderate tropical storms and hurricanes: these are more effectively moderated in the Northern Hemisphere by G4 aerosol injection and in the Southern Hemisphere by G1 solar dimming. We have no mechanism for this response, but we note that the response of TC varies between basins with notable hemispheric differences in response to G4 and rcp45 (Wang et al., submitted to ACP).

Analysis of the 1991 Pinatubo and 1982 El Chichón volcanic eruptions by Evan (2012) revealed significant reduction in TC number ($p<0.01$) in Atlantic hurricane frequency duration and intensity in the three following seasons compared with the three prior to the eruptions. This corresponds with reduced cyclogenesis in the region 8°-20°N during July-November, driven by decreases in sea surface temperatures of about 0.8°C and stratospheric warming (at 70 hPa) of about 3°C caused by the volcanic aerosol direct effect. The G4 experiment is equivalent to about one-quarter of a Pinatubo eruption, so the effects would be much weaker, consistent with the modest changes seen in Fig. 8f. The greater effectiveness of G4 stratospheric aerosol than G1 solar dimming in changing Rx5day (Fig. 8j) during July-November in the northern tropics is suggestive that both the sea surface temperature reduction and the stratospheric heating are playing significant roles in changing tropical cyclogenesis.

In summary, the normalized zonal mean annual responses in TNn, TXx and to a lesser extent for Rx5day show similar meridional structure and magnitude for solar dimming and aerosol injection geoengineering (Fig. 6h, 7h, 8h), with the exception of Northern Hemisphere high latitudes where the two geoengineering methods show different effectiveness in moderating the seasonality of TNn and TXx.

4 Summary and conclusions

We have compared the impacts of reduced solar radiation (G1) and stratospheric aerosol injection (G4) on temperature and precipitation extremes in corresponding reference experiments (abrupt4×CO_2 and rcp45, respectively), particularly their spatial and temporal patterns. Most previous studies comparing solar dimming and stratospheric aerosol SRM have concentrated on the climate mean response (Jones et al., 2011; Niemeier et al., 2013; Ferraro et al., 2014). Curry et al. (2014) examined the effect of G1 geoengineering on the same metrics of extreme temperature and precipitation response (both magnitude and duration) as examined here, but did not compare the responses of solar dimming and stratospheric aerosol injection that we focus on in this paper.

Despite large difference in the magnitude of the response induced by the two geoengineering schemes (which is somewhat larger than the ratio of the input forcings), our results show that the patterns of extreme high and low temperature in solar dimming SRM and aerosol injection SRM are geographically similar, with only small regional differences. Solar dimming SRM is relatively more effective in reducing night-time temperatures (TNn) in high-latitude summer, especially in the Arctic. There are much smaller differences in the effectiveness of aerosol and dimming SRM for the warmest day (TXx), though high latitude winters are more affected by aerosols than solar dimming as may be expected due to the absence of sunlight.

As reflected by the wettest consecutive five days index Rx5day, both SRM methods have a moderating effect on extreme precipitation during the hurricane/typhoon seasons for both hemispheres. Aerosol injection is more effective at reducing precipitation during the Northern Hemisphere TC season, while months outside the hurricane season are wetter under solar dimming, and vice versa in the Southern Hemisphere. Despite their different responses, both G1 and G4 moderate Rx5day in the cyclone season while increasing it other months, thus both schemes affect tropical cyclogenesis. Relative differences under both SRM methods are larger in precipitation extremes than for temperature extremes. This may be because, in addition to the cooling of sea surface temperatures facilitated by both solar dimming and aerosol injection, aerosol injection heats the stratosphere via the aerosol direct effect. This mechanism is present in all models analyzed here. This finding suggests that models that rely only on parameterizing hurricane numbers and intensity by surface temperatures (Moore et al., 2015) are likely to underestimate the impact of aerosol geoengineering compared with comparable amounts of solar dimming, though there are very large differences in how both greenhouse gas warming and aerosol injection affects cyclogenesis across the different tropical basins (Wang et al., submitted to ACP).

Davis et al (2016) and Smyth (2017) examined the changes in the mean state of the tropical Hadley cells to GHG forcing and the G1 scenario. They note that the poleward expansion of the Hadley cell occurs under the GHG forcing, but under G1 it is indistinguishable from the preindustrial control state, and moreover find that the ITCZ is reduced in its seasonal migration amplitude under G1 but not GHG forcing. Further analysis of the Hadley and Walker cell intensities under G1 (Guo et al., submitted to ACP) shows that the Hadley circulation is reduced under G1 relative to piControl, but that changes under

GHG forcing are rather more complex, affecting also the higher latitude Ferrel cells. Thus, some of the relative differences seen in the extreme indices around the tropics may reflect a tendency of geoengineering to mitigate changes in the Hadley cell caused by GHG forcing.

Compared with solar dimming SRM, aerosol SRM has larger differences between models and a much lower signal-to-noise ratio, although the aerosol geoengineering applied was of a much smaller magnitude than the solar dimming. Aerosol SRM was relatively less effective in increasing cold spell duration and decreasing warm spell duration in equatorial oceans than solar dimming, consistent with a relatively smaller cooling effect in coldest day and warmest night in equatorial oceans than in adjacent regions. The reduced cooling effect in equatorial oceans in aerosol SRM may result from the smaller reduction in shortwave radiation flux at the top of atmosphere in aerosol SRM in these regions.

Climate extremes are more readily perceived by society and can have more immediate economic and social impacts than changes in mean climate (IPCC, 2012). Yet, the ETCCDI extreme climate indices may not reflect what are considered "extreme events" by the general public. These would include events such as typhoons, severe heatwaves etc., that may occur much less frequently, but are of higher intensity, than the thresholds represented by the indices used here. The downscaling and impact modelling required to assess geoengineered climate effects has so far been limited to a study of Atlantic hurricane storm surge size and frequency (Moore et al., 2015), but such studies are a clear focus of ongoing research. More climate models with various aerosol parameterization schemes are certainly needed to describe the extreme tails of simulated climate variables. These extremes are incompletely sampled from 40-year long periods of model runs, but may be explored more thoroughly by specific impact models driven by the thermodynamic state of the climate system (Emanuel, 2013), and by planned extensions to the G1 experiment outlined under GeoMIP6 (Kravitz et al., 2015).

Acknowledgements

We thank all participants of the Geoengineering Model Intercomparison Project and their model development teams, the CLIVAR/WCRP Working Group on Coupled Modelling for endorsing GeoMIP, and the scientists managing the Earth System Grid data nodes who have assisted with making GeoMIP output available. Research was funded by the National Basic Research Program of China grant number 2015CB953600. HK and SW were supported by the SOUSEI Program, MEXT, Japan. CC is supported by the NSERC-funded Canadian Sea Ice and Snow Evolution Network. HM was supported by Research Council of Norway grant 229760/E10, and Sigma2 HPC resources hexagon and norstore (accounts nn9812k, nn9448k, NS9033K). MIROC-ESM simulations were conducted using the Earth Simulator. We thank Andy Jones for model development and comments on the manuscript. The Pacific Northwest National Laboratory is operated for the U.S. Department of Energy by Battelle Memorial Institute under contract DE-AC05-76RL01830.

References

Ahlm, L., Jones, A., Stjern, C. W., Muri, H., Kravitz, B., and Kristjánsson, J. E.: Marine cloud brightening – as effective without clouds, Atmos. Chem. Phys., 17, 13071-13087, doi: 10.5194/acp-17-13071-2017, 2017.

Arora, V. K., Scinocca, J. F., Boer, G. J., Christian, J. R., Denman, K. L., Flato, G. M., Kharin, V. V., Lee, W. G., and Merryfield, W. J.: Carbon emission limits required to satisfy future representative concentration pathways of greenhouse gases, Geophys. Res. Lett., 38, L05805, 2011.

Aswathy, V. N., Boucher, O., Quaas, M., Niemeier, U., Muri, H., Mülmenstädt, J., and Quaas, J.: Climate extremes in multi-model simulations of stratospheric aerosol and marine cloud brightening climate engineering, Atmos. Chem. Phys., 15, 9593–9610, doi:10.5194/acp-15-9593-2015, 2015.

Bala, G., Duffy, P. B., and Taylor, K. E.: Impact of geoengineering schemes on the global hydrological cycle, Proc. Natl. Acad. Sci., 105,7664–7669, doi:10.1073/pnas.0711648105, 2008.

Berdahl, M., Robock, A., Ji, D., Moore, J., Jones, A., Kravitz, B., and Watanabe, S.: Arctic cryosphere response in the Geoengineering Model Intercomparison Project (GeoMIP) G3 and G4 scenarios, J. Geophys. Res. –Atmos., 119, 1308-1321, doi: 10.1002/2013JD020627, 2014.

Bentsen, M., Bethke, I., Debernard, J. B., Iversen, T., Kirkevåg, A., Seland, Ø., Drange, H., Roelandt, C., Seierstad, I. A., Hoose, C., and Kristjánsson, J. E.: The Norwegian Earth System Model, NorESM1-M – Part 1: Description and basic evaluation of the physical climate, Geosci. Model Dev., 6, 687-720, https://doi.org/10.5194/gmd-6-687-2013, 2013.

Budyko, M. I.: Climatic Changes, American Geophysical Union, Washington D.C. 1977.

Collins, W. J., Bellouin, N., Doutriaux-Boucher, M., Gedney, N., Halloran, P., Hinton, T., Hughes, J., Jones, C. D., Joshi, M., Liddicoat, S., Martin, G., O'Connor, F., Rae, J., Senior, C., Sitch, S., Totterdell, I., Wiltshire, A., and Woodward, S.: Development and evaluation of an Earth-System model – HadGEM2, Geosci. Model Dev., 4, 1051-1075, doi:10.5194/gmd-4-1051-2011, 2011.

Corlett, R. T.: Impacts of warming on tropical lowland rainforests, Trends Ecol. Evol., 26, 606–613, doi:10.1016/j.tree.2011.06.015, 2011.

Crutzen, P. J.: Albedo enhancement by stratospheric sulfur injections: a contribution to resolve a policy dilemma? Clim. Chang., 77, 211–219, doi:10.1007/s10584-006-9101-y, 2006.

Curry, C. L., Sillmann, J., Bronaugh, D., Alterskjaer, K., Cole, J.N. S., Ji, D., Kravitz, B., Kristjánsson, J. E., Moore, J. C., Muri, H., Niemeier, U., Robock, A., Tilmes, S., and Yang, S.: A multimodel examination of climate extremes in an idealized geoengineering experiment, J. Geophys. Res. -Atmos., 3900–3923, doi:10.1002/2013JD020648, 2014.

Davis, N. A., Seidel, D. J., Birner, T., Davis, S. M., and Tilmes, S.: Changes in the width of the tropical belt due to simple radiative forcing changes in the GeoMIP simulations, Atmos. Chem. Phys., 16, 10083-10095, doi:10.5194/acp-16-10083-2016, 2016.

Dagon, K., and Schrag, D. P.: Regional climate variability under model simulations of solar geoengineering, J. Geophys. Res. –Atmos., 122, doi:10.1002/2017JD027110, 2017.

Diffenbaugh, N. S., Pal, J. S., Giorgi, F., and Gao, X. J.: Heat stress intensification in the Mediterranean climate change hotspot, Geophys. Res. Lett., 34, L11706, doi:10.1029/2007GL030000, 2007.

Donat, M. G., Alexander, L. V., Yang, H., Durre, I., R. Vose, and Caesar, J.: Global land-based datasets for monitoring climatic extremes, Bull. Am. Meteor. Soc., 94, 997-1006, doi:10.1175/BAMS-D-12-00109.1, 2013.

Emanuel, K. A.: Downscaling CMIP5 climate models shows increased tropical cyclone activity over the 21st century, PNAS, 110, 12219-12224, doi:10.1073/pnas.1301293110, 2013.

Evan, A. T.: Atlantic hurricane activity following two major volcanic eruptions, J. Geophys. Res., 117, D06101, doi:10.1029/2011JD016716, 2012.

Ferraro, A. J., Highwood, E. J., and Charlton-Perez, A. J.: Weakened tropical circulation and reduced precipitation in response to geoengineering, Environ. Res. Lett., 9, doi:10.1088/1748-9326/9/1/014001, 2014.

Frich, P., Alexander, L. V., Della-Marta, P., Gleason, B., Haylock, M., Tank, A., and Peterson, T.: Observed coherent changes in climatic extremes during the second half of the twentieth century, Clim. Res., 19, 193–212, doi:10.3354/cr019193, 2002.

Guo, A., Moore, J. C., Ji, D.: Tropical atmospheric circulation response to the G1 sunshade geoengineering radiative forcing experiment (Submitted to Atmos. Chem. Phys.)

Hong, Y., Moore, J. C., Jevrejeva, S., Ji, D., Phipps, S. J., Lenton, A., Tilmes, S., Watanabe, S. and Zhao, L.: Impact of the GeoMIP G1 sunshade geoengineering experiment on the Atlantic meridional overturning circulation, Environ. Res. Lett. 12, 034009, doi: 10.1088/1748-9326/aa5fb8, 2017.

IPCC, Managing the Risks of Extreme Events and Disasters to Advance Climate Change Adaptation, A Special Report of Working Groups I and II of the Intergovern mental Panel on Climate Change, Cambridge Univ. Press, Cambridge and New York ,2012.

Irvine, P. J., Ridgwell, A., and Lunt, D. J.: Assessing the regional disparities in geoengineering impacts, Geophys. Res. Lett., 37, 1–6, doi:10.1029/2010GL044447, 2010.

James, A. S. and Simmonds, I.: The central role of diminishing sea ice in recent Arctic temperature amplification, Nature, 464, 1334–1337, doi:10.1038/nature09051, 2010.

Ji, D., Wang, L., Feng, J., Wu, Q., Cheng, H., Zhang, Q., Yang, J., Dong, W., Dai, Y., Gong, D., Zhang, R.-H., Wang, X., Liu, J., Moore, J. C., Chen, D., and Zhou, M.: Description and basic evaluation of Beijing Normal University Earth System Model (BNU-ESM) version 1, Geosci. Model Dev., 7, 2039-2064, doi:10.5194/gmd-7-2039-2014, 2014.

Jones, A., Haywood, J., and Boucher, O.: A comparison of the climate impacts of geoengineering by stratospheric SO_2 injection and by brightening of marine stratocumulus cloud, Atmos. Sci. Lett., 12, 176–183, doi:10.1002/asl.29, 2011.

Jones, A., Haywood, J. M., Alterskjaer, K., Boucher, O., Cole, J. N. S., Curry, C. L., Irvine, P. J., Ji, D., Kravitz, B., Egill Kristjánsson, J., Moore, J. C., Niemeier, U., Robock, A., Schmidt, H., Singh, B., Tilmes, S., Watanabe, S., and Yoon, J.-H.: The impact of abrupt suspension of solar radiation management (termination effect) in experiment G2 of the Geoengineering Model Intercomparison Project (GeoMIP), J. Geophys. Res. -Atmos., 118, 9743– 9752, doi:10.1002/jgrd.50762, 2013.

Jones, P. W.: First- and second-order conservative remapping schemes for grids inspherical coordinates, Mon. Weather Rev., 127, 2204–2210, doi:10.1175/1520-0493, 1999.

Joshi, M. M., Gregory, J. M., Webb, M. J., Sexton, D. M. H., and Johns, T. C.: Mechanisms for the land/sea warming contrast exhibited by simulations of climate change, Clim. Dyn., 30, 455–465, doi:10.1007/s00382-007-0306-1, 2008.

Kravitz, B., Robock, A., Boucher, O., Schmidt, H., Taylor, K. E., G. Stenchikov, and Schulz, M.: The Geoengineering Model Intercomparison Project (GeoMIP), Atmos. Sci. Let., doi:10.1002/asl.316, 2011.

Kravitz, B., Robock, A., Forster, P. M., Haywood, J. M., Lawrence, M. G., and Schmidt, H.: An overview of the Geoengineering Model Intercomparison Project (GeoMIP), J. Geophys. Res. -Atmos., 118, 13103–13107, doi:10.1002/2013JD020569, 2013a.

Kravitz, B., Caldeira, K., Boucher, O., Robock, A., Rasch, P. J., Alterskjær, K., Karam, D. B., Cole, J. N. S., Curry, C. L., Haywood, J. M., Irvine, P. J., Ji, D., Jones, A., Kristjánsson, J. E., Lunt, D. J., Moore, J. C., Niemeier, U., Schmidt, H., Schulz, M., Singh, B. Tilmes, S., Watanabe, S., Yang, S., and Yoon, J.: Climate model response from the geoengineering model intercomparison project (GeoMIP), J. Geophys. Res. -Atmos., 118, 8320-8332. doi:10.1002/jgrd.50646, 2013b.

Kravitz, B., Forster, P. M., Jones, A., Robock, A., Alterskjær, K., Boucher, O., Jenkins, A. K. L., Korhonen, H., Kristjánsson, J. E., Muri, H., Niemeier, U., Partanen, A., Rasch, P. J., Wang, H., and Watanabe, S.: Sea spray geoengineering experiments in the geoengineering model intercomparison project (GeoMIP): Experimental design and preliminary results, J. Geophys. Res. -Atmos., 118, 11175–11186, doi:10.1002/jgrd.50856, 2013c.

Kravitz, B., Robock, A., Tilmes, S., Boucher, O., English, J. M., Irvine, P. J., Jones, A., Lawrence, M. G., MacCracken, M., Muri, H., Moore, J. C., Niemeier, U., Phipps, S. J., Sillmann, J., Storelvmo, T., Wang, H., and Watanabe, S.: The Geoengineering Model Intercomparison Project Phase 6 (GeoMIP6): Simulation design and preliminary results, Geosci. Model Dev., 8, 3379-3392, doi:10.5194/gmd-8-3379-2015, 2015.

Lau, W. K.-M., Wu, H.-T. and Kim, K.-M.: A canonical response of precipitation characteristics to global warming from CMIP5 models, Geophys. Res. Lett., 40, 3163–3169, doi:10.1002/grl.50420, 2013.

Mautner, M.: Deep-space solar screens against climatic warming: technical and research requirements, in: Space Utilization and Applications in the Pacific, Proceedings of the Third Pacific Basin International Symposium on Advances in Space Science, Technology and Applications, American Astronautical Society, Los Angeles, 711, 1989.

Meinshausen, M., Smith, S. J., Calvin, K. et al. The RCP greenhouse gas concentrations and their extensions from 1765 to 2300, Climatic Change, 109:213, doi:10.1007/s10584-011-0156-z, 2011.

Moore, J. C., Rinke, A., Yu, X., Ji, D., Cui, X., Li, Y., Alterskjær, K., Kristjánsson, J. E., Muri, H., Boucher, O., Huneeus, N., Kravitz, B., Robock, A., Niemeier, U., Schulz, M., Tilmes, S., Watanabe, S., Yang, S.: Arctic sea ice and atmospheric circulation under the GeoMIP G1 scenario, J. Geophys. Res. - Atmos., 119, 567–583, doi:10.1002/2013JD021060, 2014.

Moore, J. C., Grinsted, A., Guo, X., Yu, X., Jevrejeva, S., Rinke, A., Cui, X., Kravitz, B., Lenton, A., Watanabe, S., and Ji, D.: Atlantic hurricane surge response to geoengineering. Proceedings of the National Academy of Sciences, PNAS, 112, 13794-13799, doi:10.1073/pnas.1510530112, 2015.

Orlowsky, B., and Seneviratne, S. I.: Global changes in extreme events: regional and seasonal dimension, Clim. Change, 110, 669–696, doi:10.1007/s10584-011-0122-9, 2012.

Pithan, F. and Mauritsen, T.: Arctic amplification dominated by temperature feedbacks in contemporary climate models, Nature Geoscience, 7, 181-184, doi:10.1038/NGEO2071, 2014.

Phipps, S. J., Rotstayn, L. D., Gordon, H. B., Roberts, J. L., Hirst, A. C., and Budd, W. F.: The CSIRO Mk3L climate system model version 1.0 – Part 1: Description and evaluation, Geosci. Model Dev., 4, 483-509, doi:10.5194/gmd-4-483-2011, 2011.

Radinović, D., and Ćurić, M.: Criteria for heat and cold wave duration indexes, Theor. Appl. Climatol., 107, 505-510, doi:10.1007/s00704-011-0495-8, 2012.

Robock, A., Oman, L., and Stenchikov, G. L.: Regional climate responses to geoengineering with tropical and Arctic SO2 injections, J. Geophys. Res., 113, D16101, doi:10.1029/2008JD010050, 2008.

Sanderson, B., Tebaldi, C., and O'Neill, B.: What would it take to achieve the Paris temperature targets?, *Geophys. Res. Lett.*, 43, 7133–7142, doi:10.1002/2016GL069563, 2016.

Schmidt, H., Alterskjær, K., Bou Karam, D., Boucher, O., Jones, A., Kristjánsson, J. E., Niemeier, U., Schulz, M., Aaheim, A., Benduhn, F., Lawrence, M., and Timmreck, C.: Solar irradiance reduction to counteract radiative forcing from a quadrupling of CO2: climate responses simulated by four earth system models, Earth Syst. Dynam., 3, 63–78, doi:10.5194/esd-3-63-2012, 2012.

Seneviratne, S. I., Koster, R. D., Guo, Z., Dirmeyer, P. A., Kowalczyk, E., Lawrence, D., Liu, P., Mocko, D., Lu, C., Oleson, K. W., and Verseghy, D.: Soil moisture memory in AGCM simulations: Analysis of Global Land- Atmosphere Coupling Experiment (GLACE) data, J. Hydrometeor., 7, 1090–1112, doi:10.1175/JHM533.1, 2006.

Seneviratne, S. I., Nicholls, N., Easterling, D., Goodess, C. M., Kanae, S., Kossin, J., Luo, Y., Marengo, J., McInnes, K., Rahimi, M., Reichstein, M., Sorteberg, A., Vera, C., and Zhang, X.: Changes in climate extremes and their impacts on the natural physical environment. In: IPCC Special Report on Extremes, 109-230, 2012.

Sillmann, J., Kharin, V. V., Zhang, X., Zwiers, F. W., and Bronaugh, D.: Climate extremes indices in the CMIP5 multimodel ensemble: Part 1. Model evaluation in the present climate, J. Geophys. Res. -Atmos., 118, 1716–1733, doi:10.1002/jgrd.50203, 2013a.

Sillmann, J., Kharin, V. V., Zwiers, F. W., Zhang X., and Bronaugh, D.: Climate extremes indices in the CMIP5 multimodel ensemble: Part 2. Future climate projections, J. Geophys. Res. Atmos., 118, 2473–2493, doi:10.1002/jgrd.50188, 2013b.

Stjern, C. W., Muri, H., Ahlm, L., Boucher, O., Cole, J. N. S., Ji, D., Jones, A., Haywood, J., Kravitz, B., Lenton, A., Moore, J. C., Niemeier, U., Phipps, S. J., Schmidt, H., Watanabe, S., and Kristjánsson, J. E.: Response to marine cloud brightening in a multi-model ensemble, Atmos. Chem. Phys., doi: 10.5194/acp-2017-629.

Stocker, T. F., Qin, D., Plattner, G.-K., Tignor, M., Allen, M. K., Boschung, J., Nauels, A., Xia, Y., Bex, V., and Midgley, P. M.: IPCC, 2013: Climate Change 2013: The Physical Science Basis. Contribution of Working Group I to the Fifth Assessment Report of the Intergovernmental Panel on Climate Change, Cambridge University Press, Cambridge, United Kingdom and New York, NY, USA, 1535 pp., 2013.

Sutton, R. T., Dong, B. W., and Gregory, J. M.: Land/sea warming ratio in response to climate change: IPCC AR4 model results and comparison with observations, Geophys. Res. Lett., 34, L02701, doi:10.1002/wcc.147, 2007.

Taylor, K. E., Stouffer, R. J., and Meehl, G. A.: An Overview of CMIP5 and the Experiment Design, B. Am. Meteorol. Soc., 93, 485–498, doi:10.1175/BAMS-D-11-00094.1, 2012.

Tebaldi, C., Hayhoe, K., Arblaster, J. M., and Meehl, G. A.: Going to extremes: An intercomparison of model-simulated historical and future changes in extreme events, Clim. Change, 79, 185–211, doi:10.1007/s10584-006-9051-4, 2006.

Tilmes, S., Garcia, R. R., Kinnison, D. E., Gettelman, A., and Rasch, P. J.: Impact of geoengineered aerosols on the troposphere and stratosphere, J. Geophys. Res., 114, D12305, doi:10.1029/2008JD011420, 2009.

Tilmes, S., Fasullo, J., Lamarque, J.-F., Marsh, D. R., Mills, M., Alterskjaer, K., Muri, H., Kristjánsson, J. E., Boucher, O., Schulz, M., Cole, J. N. S., Curry, C. L., Jones, A., Haywood, J., Irvine, P. J., Ji, D., Moore, J. C., Karam, D. B., Kravitz, B., Rasch, P. J., Singh, B., Yoon, J.-H., Niemeier, U., Schmidt, H., Robock, A., Yang, S., and Watanabe, S.: The hydrological impact of geoengineering in the

Geoengineering Model Intercomparison Project (GeoMIP), J. Geophys. Res. -Atmos., 118, 11,036–11,058, doi:10.1002/jgrd.50868, 2013.

Tilmes, S., Jahn, A., Kay, J. E., Holland, M., and Lamarque, J.-F.: Can regional climate engineering save the summer Arctic sea ice? Geophys. Res. Lett., 41, 880–885, doi:10.1002/2013GL058731, 2014.

Volodin, E. M., Kostrykin, S. V., and Ryaboshapko, A. G.: Climate response to aerosol injection at different stratospheric locations, Atmos. Sci. Let., 12, 381-385, doi:10.1002/asl.351, 2011.

Watanabe, S., Hajima, T., Sudo, K., Nagashima, T., Takemura, T., Okajima, H., Nozawa, T., Kawase, H., Abe, M., Yokohata, T., Ise, T., Sato, H., Kato, E., Takata, K., Emori, S., and Kawamiya, M.: MIROC-ESM 2010: model description and basic results of CMIP5-20c3m experiments, Geosci. Model Dev., 4, 845-872, doi:10.5194/gmd-4-845-2011, 2011.

Yu, X., Moore, J. C., Cui, X., Rinke, A., Ji, D., Kravitz, B., and Yoon, J.-H.: Impacts, effectiveness and regional inequalities of the GeoMIP G1 to G4 solar radiation management scenarios, Global Planet Change, 129, 10-22, doi:10.1016/j.gloplacha.2015.02.010, 2015.

Wang, Q., Moore, J. C. and Ji, D.: A statistical examination of the effects of stratospheric sulphate geoengineering on tropical storm genesis, (Submitted to Atmos. Chem. Phys.)

Zhang, X., Alexander, L., Hegerl, G. C., Jones, P., Tank, A. K., Peterson, T. C., Trewin, B., and Zwiers, F. W.: Indices for monitoring changes in extremes based on daily temperature and precipitation data, WIREs Clim. Change, 2, 851–870, doi:10.1002/wcc.147, 2011.

Atmos. Chem. Phys. Discuss., https://doi.org/10.5194/acp-2018-131
Manuscript under review for journal Atmos. Chem. Phys.
Discussion started: 15 March 2018

Table 1: GeoMIP Models used in this study

No.	Model	Institution	Resolution (Lon×Lat Level)
1	BNU−ESM (Ji et al. 2014)	Beijing Normal University, China	2.8°×2.8° L26
2	CanESM2 (Arora et al., 2011)	Canadian Centre for Climate Modelling, Canada	2.8°×2.8° L35
3	GISS-E2-R (Schmidt et al. 2011)	Goddard Institute for Space Studies, USA	2.5°×2.0° L40
4	HadGEM2−ES (Collins et al. 2011)	Met Office Hadley Centre, UK	1.875°×1.25° L40
5	MIROC−ESM (Watanabe et al. 2011)	AORI, NIES, JAMSTEC, Japan	2.8°×2.8° L80
6	NorESM1-M (Bentsen et al. 2013)	University of Oslo, Norway	1.9°x2.5° L26

Table 2: Indices of climate extremes

Index	Description	Definition	Units
TNn	Coldest daily Tmin	Annual minimum value of daily minimum temperature	℃
TXx	Warmest daily Tmax	Annual maximum value of daily maximum temperature	℃
Rx5day	Wettest consecutive five days	Maximum of consecutive 5-day (cumulative) precipitation amount	mm
CSDI	Cold spell duration	Number of consecutive days (> 6 days) when daily minimum temperature falls below the 10th percentile of piControl	days
WSDI	Warm spell duration	Number of consecutive days (> 6 days) when daily maximum temperature falls above the 90th percentile of piControl	days
CDD	Consecutive dry days	Maximum number of consecutive days when precipitation < 1 mm	days

Table 3: Differences and ratios in means and climate extreme indices over the 40-year analysis period.

Experiments	Indices	Land	Ocean	Global
G1 − abrupt4 × CO2	TNn(°C)	-6.4	-4.5	-5.1
	TXx(°C)	-6.2	-3.7	-4.4
	Rx5day(mm)	-12.3	-13.4	-13.1
	SW flux(Wm^{-2})	-12.6	-10.5	-11.1
	Mean T(°C)	-5.6	-3.7	-4.3
	Mean P(mm a^{-1})	-81.0	-106.4	-98.9
G4 − rcp45	TNn(°C)	-0.9	-0.6	-0.7
	TXx(°C)	-0.8	-0.5	-0.6
	Rx5day(mm)	-1.6	-1.9	-1.8
	SW flux(Wm^{-2})	-2.0	-1.6	-1.7
	Mean T(°C)	-0.7	-0.5	-0.5
	Mean P(mm a^{-1})	-8.2	-16.6	-14.1
$\frac{\text{G1} - \text{abrupt4} \times \text{CO2}}{\text{G4} - \text{rcp45}}$	TNn	6.9	7.6	7.3
	TXx	7.5	7.7	7.6
	Rx5day	7.8	7.2	7.3
	SW flux	6.4	6.6	6.5
	Mean T	7.9	8.3	8.1
	Mean P	9.8	6.4	7.0